Magazine of Civil Engineering

ISSN 2071–0305

journal homepage: http://engstroy.spbstu.ru/

DOI: 10.18720/MCE.95.3

Stability of fixed-fixed shallow arches under arbitrary radial and vertical forces

L.P. Kiss*
Institute of Applied Mechanics, University of Miskolc, Miskolc, Hungary
** E-mail: mechkiss@uni-miskolc.hu*

Keywords: buckling, stiffness, strength, design, composite materials

Abstract. In the present paper the planar stability of fixed-fixed shallow circular arches is investigated. The arches are made of linearly elastic, functionally graded material and are subject to a concentrated radial or vertical dead force at an arbitrary position. To describe the behaviour, the one-dimensional Euler-Bernoulli kinematic hypothesis is used. The effect of the bending moment on the membrane strain is incorporated into the model. The related coupled differential equations of the problem are derived from the principle of virtual work. Exact solutions are found both for the pre- and post-bucking displacements. Closed-form analytical solution is given for the buckling load when the load is radial while for vertical force, the solution is numerical. It is found that for fixed-fixed members, only limit point buckling is possible. Such shallow arches are not sensitive to small imperfections in the load position or in the load direction. It turns out that the material composition and geometry have significant effects on the behaviour and buckling load. If the load is placed far enough from the crown point, the load bearing abilities become better than for crown-load. Comparisons with an analytical literature model and commercial finite element software confirm the validity of the new findings.

1. Introduction

Curved members (arches, shells) are often used in engineering applications, e.g., in aerospace structures or in civil engineering structures [1, 2]. These elements are preferred because of their advantageous mechanical behaviour under various loading conditions and partially because of their favourable design.

Compared to classical homogeneous materials, composites have such advantageous properties like the increased durability or reduced weight [3–5]. Functionally graded materials (FGM) have a further notable benefit, that is the smooth stress distribution because of the continuously changing material properties. For these previous reasons, such composite materials are being used more and more frequently [6–9] by civil engineers. Thus, it is important to be able to predict the mechanical behaviour of such members.

Buckling is a well-known phenomenon, which can occur for various structural members [10–12]. Thus, the in-plane stability of arches is not a new topic as there is a bunch of available works, like [13–15] in the open literature. It is well-known that their behaviour is nonlinear since the pre-buckling deformations are significant. There are many arch problems that have been solved either analytically or by means of a numerical method [16–22]. These issues involve the effect of the foundation stiffness, remote unconnected equilibria, inclusion of geometric imperfections, elastic horizontal and rotational end restraints. The preferred numerical methods include the analog equation method, the modified Riks method and the Galerkin method as well.

Studies [23–27] report about analytical solutions on the stability of shallow arches with multiple stiffness regions along the centroidal axis. The Euler-Bernoulli hypothesis is considered and various load and support conditions are investigated. Articles [28–30] focus on FGM arches analytically using the classical shallow arch theory.

It is found that simple crown-point loads are preferred in the literature. However, in practice, other load positions are also possible. Early articles [31, 32] investigate the effect of the load position on arches but the later one neglects the effect of the axial compressive force. There is a recent article series about the in-plane stability of arches under arbitrary concentrated radial load [33–35] by using the same hypotheses as in [36–37]. These works present analytical investigations for homogeneous material but the effect of the bending

Kiss, L.P. Stability of fixed-fixed shallow arches under arbitrary radial and vertical forces. Magazine of Civil Engineering. 2020. 95(3). Pp. 31–41. DOI: 10.18720/MCE.95.3

moment on the membrane strain is neglected. An improved kinematical hypothesis is presented and evaluated in the likes of [38–40].

According to the literature review, it is an open question how fixed-fixed FGM shallow arches behave under a radial or vertical dead load at an arbitrary position. The aim of the current article is to find the answer to this issue. The related tasks, therefore, are:

1. to introduce a new geometrically nonlinear beam model, incorporating the effect of the bending moment on the membrane strain;
2. to find the related static equilibrium equations using a suitable variational principle and to solve these coupled equations in closed-form;
3. to derive the buckling equations and investigate the possibility and conditions of bifurcation and limit point buckling;
4. to show the effect of various geometrical and material parameters on the buckling load;
5. to verify the outcomes, i.e., compare the new results with the literature and finite element computations.

2. Methods

2.1. Kinematics

A fixed-fixed shallow FG circular arch is considered. Its (E-weighted) centroidal axis is shown in Fig. 1. The axis ξ coincides with the circumferential direction, while the cross-sectional coordinates are $\eta;\zeta$. The cross-section is symmetric to ζ, i.e., η is a principal axis. The initial radius of the centroidal axis is ρ and the included angle of the arch is 2ϑ with ϕ being the angle coordinate. The external load Q is a dead concentrated force at $\phi=\alpha$ and is either radial ($\gamma=0$) or vertical ($\gamma=\alpha$). The FG material composition is a mixture of metallic (subscript m) and ceramic (subscript c) phases. The material constituents – like the Young modulus E are assumed to follow a power-law distribution (e.g., the Voigt rule of mixture) along the thickness as

$$E(\zeta)=(E_c-E_m)\left(\frac{\zeta}{b}\right)^k+E_m \tag{1}$$

with b being the height of the cross-section and k is the volume fraction index [42].

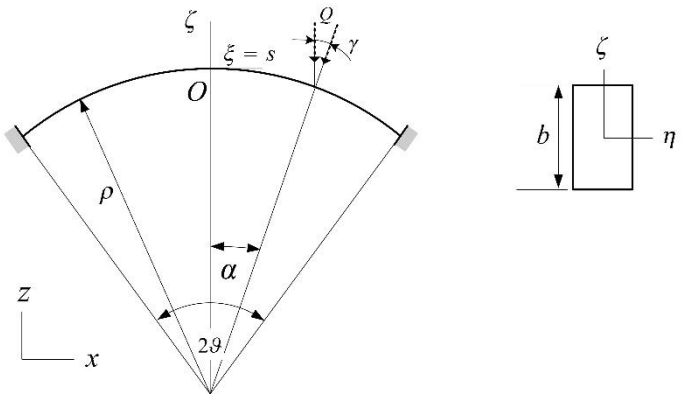

Figure 1. A fixed-fixed shallow arch with radius ρ and included angle 2ϑ under a concentrated radial/vertical load Q.

Using the Euler-Bernoulli hypothesis, the longitudinal strain at an arbitrary point is [41] expressed by

$$\varepsilon_\xi=\frac{\rho}{\rho+\zeta}\left[\frac{du}{ds}+\frac{w}{\rho}+\zeta\left(\frac{du}{\rho ds}-\frac{d^2w}{ds^2}\right)\right]+\frac{1}{2}\left(\frac{u}{\rho}-\frac{dw}{ds}\right)^2, \tag{2}$$

with the nonlinear membrane strain – $\zeta=0$ – and the cross-sectional rotation being

$$\varepsilon = \frac{du}{ds} + \frac{w}{\rho} + \frac{1}{2}\psi^2; \quad \psi = \frac{u}{\rho} - \frac{dw}{ds}. \tag{3}$$

The circumferential and lateral displacements are denoted by u and w.

According to the Hooke law, the axial force and bending moment are as follows [41]:

$$N = \int_A \sigma_\xi dA = E_1\varepsilon - \frac{E_3}{\rho}\left(\frac{1}{\rho}\frac{du}{ds} - \frac{d^2w}{ds^2}\right), \tag{4a}$$

$$M = \int_A \zeta\sigma_\xi dA = -E_3\left(\frac{d^2w}{ds^2} + \frac{w}{\rho^2}\right), \quad N + \frac{M}{\rho} = E_1\varepsilon. \tag{4b}$$

Thus, clearly, the effect of the bending moment on the membrane strain is accounted, unlike in some previous models. In the expressions of the inner forces the various stiffnesses are defined by

$$E_j = \int_A E\zeta^{j-1} dA. \tag{5}$$

At the points of the centroidal axis $E_2 = 0$.

2.1.1 Equilibrium equations

The principle of virtual work is used to find the nonlinear pre-buckling equilibrium configuration. It requires that equation

$$\int_V \sigma_\xi \delta\varepsilon_\xi \, dV - \mathbf{Q}\cdot\delta\mathbf{w}\big|_{\phi=\alpha} = 0 \tag{6}$$

to be satisfied by any kinematically admissible virtual field $\delta()$. Due to the shallowness of the arch, only the virtual work done by the external force on the radial displacement field is accounted. From the above principle, the following coupled differential equation (DE) system can be found [40]:

$$\frac{dN}{ds} + \frac{1}{\rho}\left[\frac{dM}{ds} - \left(N + \frac{M}{\rho}\right)\psi\right] = 0, \tag{7}$$

$$\frac{d}{ds}\left[\frac{dM}{ds} - \left(N + \frac{M}{\rho}\right)\psi\right] - \frac{N}{\rho} = 0. \tag{8}$$

These equations can be given in terms of the dimensionless displacement $W = w/\rho$ and the notation $d()/ds = (\,)'$ as

$$\varepsilon' = 0, \qquad W'''' + \left(\chi^2 + 1\right)W'' + \chi^2 W = \chi^2 - 1, \tag{9}$$

with the strain- and geometrical-material parameters being defined as

$$\chi^2 = 1 - \mu\varepsilon; \quad \mu = \frac{E_1\rho^2}{E_3} = \frac{\rho^2}{r^2}; \quad r^2 = \frac{E_3}{E_1}. \tag{10}$$

So, the effect of the material composition is incorporated into the model through these quantities. Furthermore, it is found that the membrane strain is constant. Equilibrium equations are comparable to, e.g., [28, 43].

Focusing now on the post-buckling equilibrium state, the typical increments – noted by a hat symbol $\hat{()}$ – are [38]

$$\hat{\varepsilon}_\xi = \frac{\rho}{\rho + \zeta}\left[\frac{d\hat{u}}{ds} + \frac{\hat{w}}{\rho} + \zeta\frac{d\hat{\psi}}{ds}\right] + \psi\hat{\psi}, \quad \hat{\psi} = \frac{\hat{u}}{\rho} - \frac{d\hat{w}}{ds}, \tag{11}$$

$$\hat{\varepsilon} = \frac{d\hat{u}}{ds} + \frac{\hat{w}}{\rho} + \left(\frac{u}{\rho} - \frac{dw}{ds} \right)\left(\frac{\hat{u}}{\rho} - \frac{d\hat{w}}{ds} \right), \tag{12}$$

$$\hat{N} = E_1 \hat{\varepsilon} - \frac{\hat{M}}{\rho}, \quad \hat{M} = -E_3 \left(\frac{d^2\hat{w}}{ds^2} + \frac{\hat{w}}{\rho^2} \right). \tag{13}$$

From the principle of virtual work for the buckled equilibrium configuration, equation

$$\int_V \sigma_\xi^* \delta\varepsilon_\xi^* \, dV - \mathbf{Q}^* \cdot \delta\mathbf{w}^* \Big|_{\phi=\alpha} = 0 \tag{14}$$

is to be satisfied. Here $()^* = () + \hat{()}$ is the sum of the pre- and post-buckling components of any quantity. The following DEs are found from this principle [41]:

$$\frac{d\hat{N}}{ds} + \frac{1}{\rho}\frac{d\hat{M}}{ds} - \frac{1}{\rho}\left(N + \frac{M}{\rho} \right)\hat{\psi} - \frac{1}{\rho}\left(\hat{N} + \frac{\hat{M}}{\rho} \right)\hat{\psi} = 0, \tag{15a}$$

$$\frac{d^2\hat{M}}{ds^2} - \frac{\hat{N}}{\rho} - \frac{d}{ds}\left[\left(N^* + \frac{M^*}{\rho} \right)\hat{\psi} + \left(\hat{N} + \frac{\hat{M}}{\rho} \right)\psi \right] = 0, \tag{15b}$$

which are actually

$$\hat{\varepsilon}' = 0, \tag{16}$$

$$\hat{W}'''' + (\chi^2 + 1)\hat{W}'' + \chi^2 \hat{W} = \mu\hat{\varepsilon}\left[1 - \left(W'' + W \right) \right], \quad \hat{W} = \hat{w}/\rho. \tag{17}$$

These results are again comparable to previous models, like [28, 44].

3. Results and Discussion

3.1. Solution – pre-buckling state

The following closed-form general solution was found to satisfy Eq. (9)$_2$

$$W_i(\phi) = \frac{\chi_i^2 - 1}{\chi_i^2} + C_{1i}\cos\phi + C_{2i}\sin\phi - \frac{C_{3i}}{\chi_i^2}\cos\chi_i\phi - \frac{C_{4i}}{\chi_i^2}\sin\chi_i\phi, \tag{18}$$

with $C_{1i} - C_{4i}$ being integration constants, χ_i being the membrane strain parameter defined by

$$\chi_i = \sqrt{1 - \mu\varepsilon_i} \tag{19}$$

and furthermore, here and now on, subscript $i = \{r, l\}$ if ϕ is $\{\geq\alpha; <\alpha\}$.

When the load is radial, the strain is constant on the whole centroidal axis while for vertical load, the strain has a jump at $\phi = \alpha$. The jump (discontinuity) magnitude is found from the variational principle as

$$\chi_l^2 = \chi_r^2 + \frac{2P\sin\gamma}{\vartheta}; \quad P = \frac{Q\rho^2\vartheta}{2E_3} \tag{20}$$

with P being a dimensionless load. Thus, the average membrane strain – recalling (19) and (20) – is

$$\bar{\varepsilon} = -\frac{1}{\mu}\frac{\left(\chi_l^2 - 1\right)\left(\vartheta + \alpha\right) + \left(\chi_r^2 - 1\right)\left(\vartheta - \alpha\right)}{2\vartheta} \tag{21}$$

with $\chi_l = \chi_r$ for radial load. As a consequence, the solution for the displacement field is sought separately on the two sides of the external load. Based on the virtual work principle, the following boundary, continuity and discontinuity conditions are valid for the arch:

$$W_l\big|_{-\vartheta} = W_l'\Big|_{-\vartheta} = W_r\big|_{\vartheta} = W_r'\Big|_{\vartheta} = 0, \tag{22}$$

$$W_l\big|_{\alpha} = W_r\big|_{\alpha} \quad W_l'\Big|_{\alpha} = W_r'\Big|_{\alpha}, \tag{23}$$

$$W_l''\Big|_{\alpha} = W_r''\Big|_{\alpha} \quad -W_l'''\Big|_{\alpha} + W_r'''\Big|_{\alpha} = -\frac{2P\cos\gamma}{\vartheta}. \tag{24}$$

All these above fields are continuous except the third derivative, which is proportional to the shear force. It has a jump for both radial and vertical load. Substituting here solutions (18), the system of linear equations is found:

$$\begin{bmatrix}
\cos\vartheta & -\sin\vartheta & -\frac{\cos\chi_l\vartheta}{\chi_l^2} & \frac{\sin\chi_l\vartheta}{\chi_l^2} & 0 & 0 & 0 & 0 \\
-\chi_l\sin\vartheta & -\chi_l\cos\vartheta & \sin\chi_l\vartheta & \cos\chi_l\vartheta & 0 & 0 & 0 & 0 \\
\cos\alpha & \sin\alpha & -\frac{\cos\chi_l\alpha}{\chi_l^2} & -\frac{\sin\chi_l\alpha}{\chi_l^2} & -\cos\alpha & -\sin\alpha & \frac{\cos\chi_r\alpha}{\chi_r^2} & \frac{\sin\chi_r\alpha}{\chi_r^2} \\
\chi_l\sin\alpha & -\chi_l\cos\alpha & -\sin\chi_l\alpha & \cos\chi_l\alpha & -\chi_r\sin\alpha & \chi_r\cos\alpha & \sin\chi_r\alpha & -\cos\chi_r\alpha \\
-\cos\alpha & -\sin\alpha & \cos\chi_l\alpha & \sin\chi_l\alpha & \cos\alpha & \sin\alpha & -\cos\chi_r\alpha & -\sin\chi_r\alpha \\
-\sin\alpha & \cos\alpha & \chi_l\sin\chi_l\alpha & -\chi_l\cos\chi_l\alpha & \sin\alpha & -\cos\alpha & -\chi_r\sin\chi_r\alpha & \chi_r\cos\chi_r\alpha \\
0 & 0 & 0 & 0 & \cos\vartheta & \sin\vartheta & -\frac{\cos\chi_r\vartheta}{\chi_r^2} & -\frac{\sin\chi_r\vartheta}{\chi_r^2} \\
0 & 0 & 0 & 0 & \chi_r\sin\vartheta & -\chi_r\cos\vartheta & -\sin\chi_r\vartheta & \cos\chi_r\vartheta
\end{bmatrix}.$$

$$\begin{bmatrix} C_{1l} \\ C_{2l} \\ C_{3l} \\ C_{4l} \\ C_{1r} \\ C_{2r} \\ C_{3r} \\ C_{4r} \end{bmatrix} = \begin{bmatrix} -\frac{\chi_l^2-1}{\chi_l^2} \\ \frac{\chi_r^2-1}{\chi_r^2} - \frac{\chi_l^2-1}{\chi_l^2} \\ 0 \\ 0 \\ 0 \\ \frac{-2P\cos\gamma}{\vartheta} \\ -\frac{\chi_r^2-1}{\chi_r^2} \\ 0 \end{bmatrix}.$$

The coefficients C_{ji} can now be calculated in closed-form.

Because of equilibrium Eq. $(9)_1$, the membrane strain is constant on the centroidal axis, so it is equal to the average membrane strain given by:

$$\varepsilon = \overline{\varepsilon} = \frac{1}{\vartheta+\alpha}\int_{-\vartheta}^{\alpha}\varepsilon_l(\phi)d\phi + \frac{1}{\vartheta-\alpha}\int_{\alpha}^{\vartheta}\varepsilon_r(\phi)d\phi = \text{constant}. \tag{25}$$

Recalling Eq. (3) and assuming $w >> u$ due to the shallowness, which is generally accepted in the literature [33], a quadratic equation in P is established for fixed-fixed shallow arches under arbitrary radial ($\chi_l = \chi_r$; $\gamma = 0$) load as:

$$G_0 + G_1 P + G_2 P^2 = 0. \tag{26}$$

The constants G_0-G_2 are functions of $\mu, \alpha, \vartheta, \chi$. This previous equation can be solved analytically for any given strain-, geometrical and material parameter.

When the load is vertical – $\chi_l \neq \chi_r$; $\gamma = \alpha$ – the above equation becomes strongly nonlinear in the dimensionless load because of Eq. (20) and

$$H_0(\mu, \alpha, \gamma, \vartheta, P, \chi_l, \chi_r) = 0 \tag{27}$$

can only be tackled numerically.

3.2. Buckled equilibrium

The general solution to the inhomogeneous post-buckling equilibrium equation (17) is

$$\hat{W}_i(\phi) = D_{1i}\cos\phi + D_{2i}\sin\phi + D_{3i}\sin\chi_i\phi + D_{4i}\cos\chi_i\phi - \frac{\mu\hat{\varepsilon}_i}{2\chi_i^3}\left(\frac{2}{\chi_i} + C_{3i}\phi\sin\chi_i\phi - C_{4i}\phi\cos\chi_i\phi\right) \tag{28}$$

with the unknown constants $D_{1i} - D_{4i}$. The related boundary and continuity conditions are

$$\hat{W}_l\big|_{-\vartheta} = \hat{W}_l'\big|_{-\vartheta} = \hat{W}_r\big|_{\vartheta} = \hat{W}_r'\big|_{\vartheta} = 0, \tag{29}$$

$$\hat{W}_l\big|_{\alpha} = \hat{W}_r\big|_{\alpha}, \quad \hat{W}_l'\big|_{\alpha} = \hat{W}_r'\big|_{\alpha}, \tag{30}$$

$$\hat{W}_l''\big|_{\alpha} = \hat{W}_r''\big|_{\alpha}, \quad \hat{W}_l'''\big|_{\alpha} = \hat{W}_r'''\big|_{\alpha} \tag{31}$$

with all the typical fields being continuous at $\phi = \alpha$ as there is no load increment ($\hat{Q} = 0$). These conditions determine an inomogeneous linear equation system which can be solved in closed-form. According to (16), the strain increment is constant, thus, with (12) and the inequality $\hat{w} >> \hat{u}$ used on (16) it is found that

$$\hat{\varepsilon} = \frac{1}{2\vartheta}\int_{-\vartheta}^{\vartheta}\left(\hat{U}' + \hat{W} + W'\hat{W}'\right)d\phi. \tag{32}$$

It is again a quadratic equation in the dimensionless load when the force is radial:

$$J_0 + J_1 P + J_2 P^2 = 0 \tag{33}$$

with $J_1; J_2; J_3$ being functions of $\mu, \alpha, \vartheta, P, \chi$ and it leads to a strongly nonlinear relationship for vertical load:

$$K_0(\mu, \alpha, \gamma, \vartheta, P, \chi_l, \chi_r) = 0. \tag{34}$$

Solution for limit point (of snap-through) buckling can be evaluated for any geometry and material distribution by solving simultaneously nonlinear Eqs. (26); (33) for radial load and (27); (34) for vertical load. Or, alternatively, since limit points are local maxima on the equilibrium path [42], the very same results can be found by differentiating Eq. (26) or (27) with respect to the strain parameter.

In theory, it is also possible for fixed-fixed shallow arches under concentrated load to undergo bifurcation buckling [38]. During bifurcation, the load and membrane strain remain constant [36] and the arch buckles to an infinitesimally close bifurcation equilibrium configuration. In this case, solution to DE (17) with $\hat{\varepsilon} = 0$ is

$$\hat{W}_i(\phi) = S_{1i}\cos\phi + S_{2i}\sin\phi + S_{3i}\sin\chi_i\phi + S_{4i}\cos\chi_i\phi. \tag{35}$$

This solution and the conditions (29)–(31) determine a homogeneous linear system of equations. Nontrivial solution exists if the determinant of the coefficient matrix vanishes, therefore

$$\begin{vmatrix}
\cos\vartheta & -\sin\vartheta & -\sin\chi_l\vartheta & \cos\chi_l\vartheta & 0 & 0 & 0 & 0 \\
\sin\vartheta & \cos\vartheta & \chi_l\cos\chi_l\vartheta & \chi_l\sin\chi_l\vartheta & 0 & 0 & 0 & 0 \\
\cos\alpha & \sin\alpha & \sin\chi_l\alpha & \cos\chi_l\alpha & -\cos\alpha & -\sin\alpha & -\sin\chi_r\alpha & -\cos\chi_r\alpha \\
-\sin\alpha & \cos\alpha & \chi_l\cos\chi_l\alpha & -\chi_l\sin\chi_l\alpha & \sin\alpha & -\cos\alpha & -\chi_r\cos\chi_r\alpha & \chi_r\sin\chi_r\alpha \\
-\cos\alpha & -\sin\alpha & -\chi_l^2\sin\chi_l\alpha & -\chi_l^2\cos\chi_l\alpha & \cos\alpha & \sin\alpha & \chi_r^2\sin\chi_r\alpha & \chi_r^2\cos\chi_r\alpha \\
\sin\alpha & -\cos\alpha & -\chi_l^3\cos\chi_l\alpha & \chi_l^3\sin\chi_l\alpha & -\sin\alpha & \cos\alpha & \chi_r^3\cos\chi_r\alpha & -\chi_r^3\sin\chi_r\alpha \\
0 & 0 & 0 & 0 & \cos\vartheta & \sin\vartheta & \chi_r^2\sin\chi_r\vartheta & \chi_r^2\cos\chi_r\vartheta \\
0 & 0 & 0 & 0 & -\sin\vartheta & \cos\vartheta & \chi_r^3\cos\chi_r\vartheta & -\chi_r^3\sin\chi_r\vartheta
\end{vmatrix} = 0$$

This determinant, in fact, yields the critical strain for bifurcation buckling. However, recalling the solutions of [33] and [38], it is clear that, for fixed-fixed shallow arches under a concentrated load, bifurcation buckling is possible only when $\alpha = 0$ and in this case, the bifurcation point is always located on the unstable equilibrium branch. It means that only limit point buckling can occur.

3.3. Analytical and numerical solutions

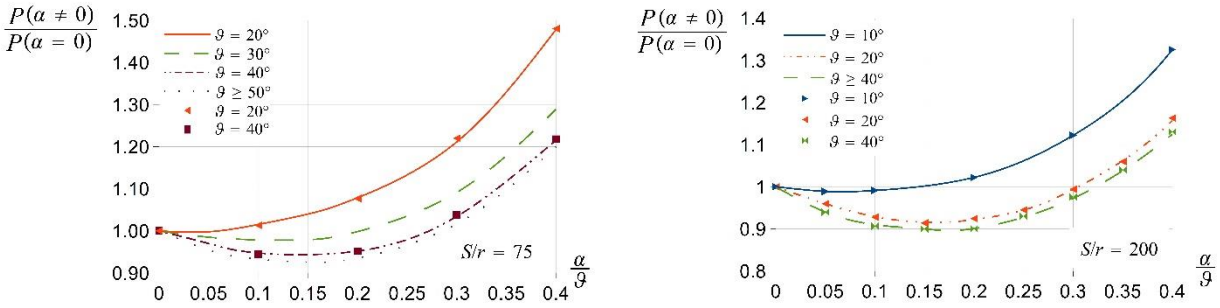

Figure 2. The critical load ratio for non-crown and crown loads in terms of the relative load position parameter α / ϑ for arches with: a – *S/r* = 75; b – *S/r* = 200.

First, the effect of the load position α on the lowest critical load is investigated for multiple semi-vertex angles ϑ. Results are plotted in Fig. 2a and 2b for two S/r ratios – S is the length of the centroidal axis and r is the *E*-weighted radius of gyration. $P(\alpha = 0)$ is the critical dimensionless load at the crown and $P(\alpha \neq 0)$ is the critical load when the force is placed elsewhere. Different line types are drawn for radial load while markers are used to show the findings for vertical force. When the load is in the small vicinity of the crown point $\alpha << 2\vartheta$ the buckling load changes (decreases) slowly for all the selected geometries. Thus, fixed-fixed arches, unlike pinned-pinned members [39], are not sensitive to small imperfections in the load position. In general, replacing the load from the crown makes the buckling load decrease for a while. Then it is always followed by an increase and if the load is exerted sufficiently far from the crown point, the load bearing abilities become better than for $\alpha = 0$. Overall, smaller included angle means smaller change in the buckling load. When $S/r = 75$, the semi-vertex angle and load position have greater effects compared to $S/r = 200$. Above a certain angle, the behaviour seems to become independent of the angle as well.

It is also found that in the investigated range it does not really matter if the load is vertical or radial, i.e., fixed-fixed shallow arches are not sensitive to small imperfections in the load direction in relation to the radial one.

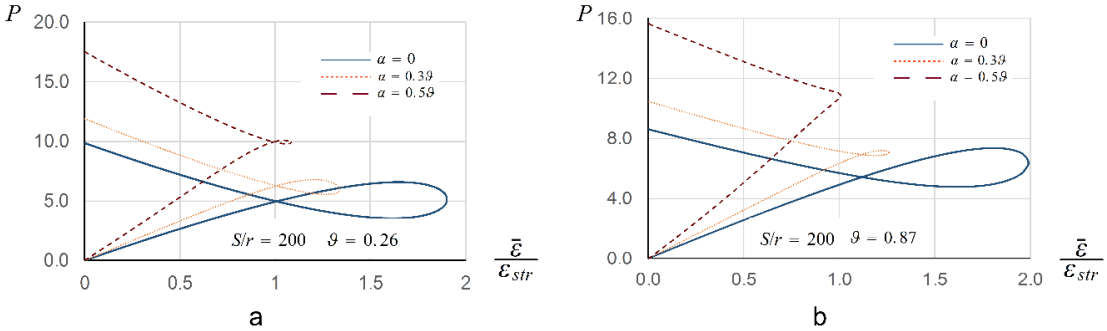

Figure 3. Dimensionless load vs membrane strain parameter to depict the effect of load position α on the behaviour of arches with *S/r=200*: a – ϑ*=0.26*; b – ϑ*=0.87.*

Next, it is investigated how the load position can affect the behaviour of arches as shown in Fig. 3a and 3b. Here, ε_{str} is the buckling strain of a straight column under compression with the same material composition, length and cross-section as the arch. Independently of the angle, it is common in the diagrams that as the strain is increased from zero, there is a possible stability loss where the tangent is horizontal. Furthermore, increasing α makes the strain ratio decrease at the moment of buckling and at the same time the dimensionless buckling load gradually becomes greater. One branch always starts from the origin and the other one from a different level. The later one is greater in the dimensionless load P if α is greater and ϑ is smaller. These diagrams are plotted for radial load but can be considered valid for vertical force also with a good accuracy.

Fig. 4-5 give information about the effect of the ratio S/r on the in-plane behaviour when the load is radial. The dimensionless displacement at the application point of the force is $W_\alpha = W(\phi = \alpha)$. As S/r decreases, the loop always becomes smaller with lower critical load and strain ratio as well. The different branches start from a same point, independently of S/r and intersect each other again at a same point as shown in Fig. 4a and 4b. This later intersection point is close to the strain ratio 1. In Fig. 5a and 5b, there are three equilibrium branches: a primary stable, a remote stable and an unstable between them. (When there is no possibility of buckling, there is only one stable branch.) It is somewhat different to pinned-pinned members [39, 40] as then, the number of equilibrium branches showed an increases with α and could reach a number quite more than three, but for fixed-fixed members the number of equilibrium branches seems to be always three. It is set down to the fact that fixed supports are stiffer. When $\alpha = 0$, the unstable branches are very flat but still there is limit point buckling at smaller dimensionless displacement compared to $\alpha = 0.2\vartheta$.

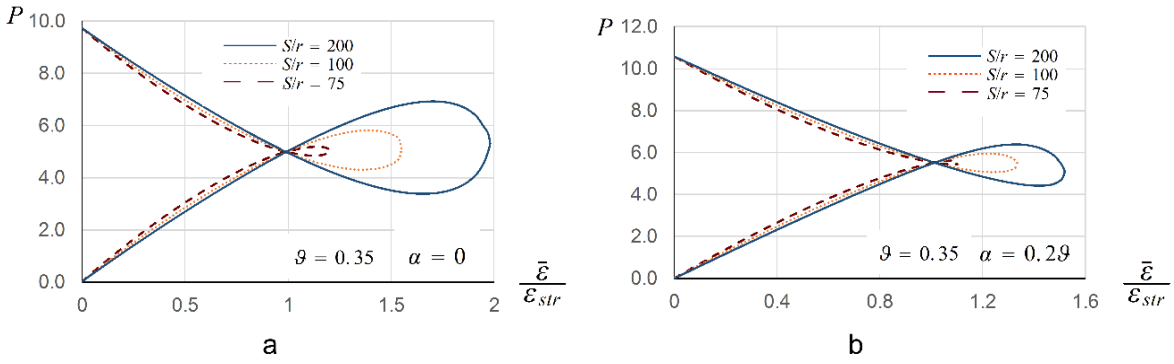

Figure 4. Dimensionless load vs membrane strain parameter to depict the effect of ratio S/r on the behaviour of arches with ϑ=0.35 when: a – α =0; b – α =0.2ϑ.

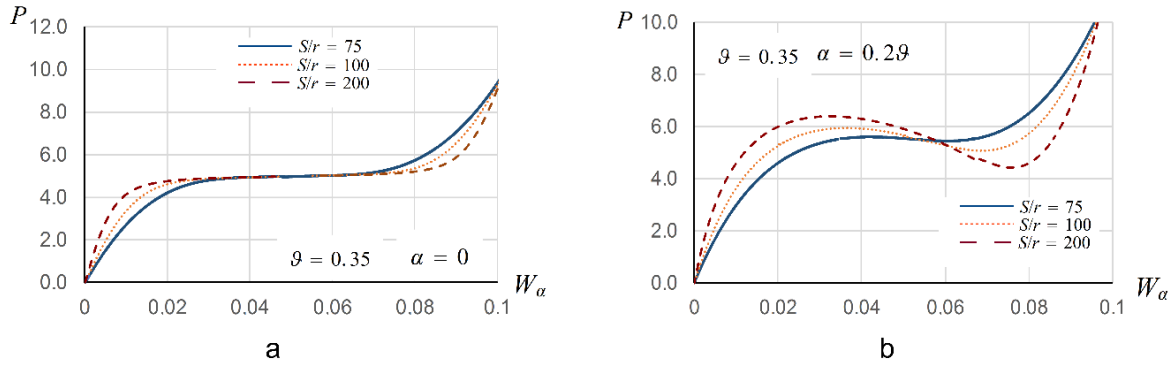

Figure 5. Dimensionless load vs dimensionless displacement at $\phi = \alpha$ to depict th effect of ratio S/r on the behaviour of arches with ϑ=0.35 when: a – α =0; b – α =0.2ϑ.

In what follows, the lowest buckling loads are plotted in terms of the included angle as shown in Fig. 6a and 6b. The various lines represent radial load and markers are used for vertical force. Clearly, the buckling load increases with S/r. It makes no real sense if the load is radial or vertical – the maximum difference between them is only a few percent at most. Increasing S/r makes the typical curves shift to the left – the possibility of buckling appears for smaller included angles.

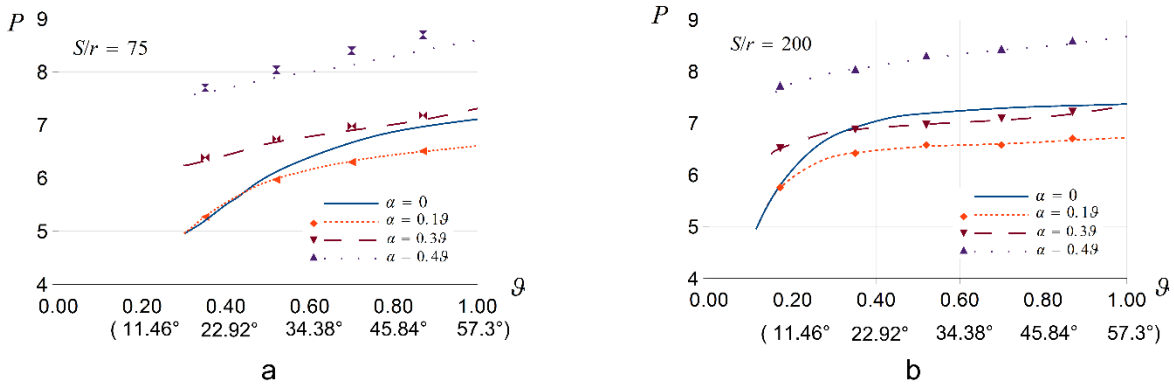

Figure 6. Lowest critical loads for multiple load positions in terms of the semi-vertex angle: a – S/r=75; b – S/r=200.

3.4. Verification of the results

For radial load, comparisons were carried out with [33] assuming homogeneous material. Results for arches with the same geometrical and material parameters are gathered in Table 1. The correlation is really good. Differences are greatest when ϑ and α are greatest. Since the new model of this article accounts for the effect of the bending moment on the membrane strain, it is assumed to be more reliable.

The new results for vertical load are also verified by the commercial finite element software Abaqus 6.13. A geometrically nonlinear model was used with the Riks method to find the limit points on the equilibrium path. A one-dimensional model was created with eighty B21 beam elements. A doubly symmetric *I*-section was selected [34]. The related geometrical data were the following: depth *256* mm, flange width *146* mm, flange thickness *10.9* mm, web thickness *6* mm. The moment of inertia is *54,255,292* mm^4 and the modulus of section is *423,869.469* mm^3 to the bending axis η while these values are *5,657,929* mm^4 and *77,505.875* mm^3 to the other principal axis ζ. So the radius of gyration r to the bending axis is *108* mm. Since $S/r = 200$ was selected, the centerline legth is *21,600* mm. The Young modulus was *210* GPa. Comparisons of the models with some further geometrical data are gathered in Table 2, indicating that the results of the current model are reliable.

Table 1. Comparison of the lowest radial dimensionless buckling loads with [33] for arches with S/r = 75 and 200.

ϑ	ρ [m]	span [m]	altitude [m]	P	P in [33]
$S/r = 75,\ \alpha = \{0/0.2/0.4\}\ \vartheta$					
0.38	10.65	7.90	0.76	5.20/5.61/7.62	5.15/5.56/7.35
0.69	5.87	7.47	1.34	6.67/6.35/8.14	6.57/6.26/7.89
1.05	3.85	6.69	1.94	7.16/6.68/8.67	7.06/6.41/7.99
$S/r = 200,\ \alpha = \{0/0.2/0.4\}\ \vartheta$					
0.38	28.42	21.08	2.03	6.92/6.38/8.05	6.92/6.37/7.97
0.69	15.65	19.92	3.58	7.29/6.54/8.42	7.28/6.49/8.05
1.05	10.28	17.84	5.17	7.39/6.76/8.74	7.34/6.51/8.07

Table 2. Comparison of the lowest dimensionless buckling loads for vertical load with Abaqus for arches with S/r=200.

ϑ	P	P, Abaqus
$S/r = 200,\ \alpha = \{0.1/0.2/0.3\}\ \vartheta$		
0.38	6.42/6.40/6.88	6.30/6.29/6.78
0.69	6.61/6.54/7.09	6.72/6.62/7.04
1.05	6.76/6.77/7.30	7.07/6.93/6.84

4. Conclusion

1. In this article a new geometrically nonlinear model was established to investigate the in-plane behaviour and stability of fixed-fixed shallow arches under the effect of a concentrated radial or vertical dead load. The arches are made of functionally graded material. The Euler-Bernoulli kinematical hypothesis was applied. Account for the effect of the bending moment on the membrane strain was made.
2. The related pre-buckling and buckled equilibrium equations were derived from the principle of virtual work. Analytical evaluations were carried our for radial load and numerical ones for vertical force.
3. It was found that only limit point buckling is possible with three equilibrium branches: two stable and one unstable for any geometry and material composition.
4. Unlike pinned-pinned arches, fixed-fixed members are not sensitive to small imperfections in the load position and in the load direction.
5. At the same time, the load position can have a significant effect on the buckling load. Generally, the buckling load decreases for a while when the force is moved from the crown point but as it is placed close enough to the supports, the load bearing abilities become even better.
6. In limit case, the presented model is also capable of predicting the buckling load for homogeneous materials.
7. The new results were confirmed by comparisons with literature and finite element computations.

5. Acknowledgements

The described article was carried out as part of the EFOP-3.6.1-16-2016-00011 „Younger and Renewing University – Innovative Knowledge City – institutional development of the University of Miskolc aiming at intelligent specialisation" project implemented in the framework of the Szechenyi 2020 program. The realization of this project is supported by the European Union, co-financed by the European Social Fund.

References

1. Gusevs, J., Serdjuks, D., Artebjakina, G., Afanasjeva, E., Goremikins, V. Behaviour of load-carrying members of velodromes' long-span steel roof. Magazine of Civil Engineering. 2016. 65(5). Pp. 3–16. DOI: 10.5862/MCE.65.1
2. Hirkovskis, A., Serdjuks, D., Goremikins, V., Pakrastins, L., Vatin, N. Behaviour analysis of load-bearing aluminium members. Magazine of Civil Engineering. 2015. 57(5). Pp. 86–117. DOI: 10.5862/MCE.57.8
3. Sharbatdar, M., Ehsani, R., Kheyroddin, A. Ductility and moment redistribution capacity of two-span RC beams. Magazine of Civil Engineering. 2019. 90(6). Pp. 104–118. DOI: 10.18720/MCE.90.10
4. Duc, N.D., Cong, P.H., Tuan, N.D., Tran, P., Thanh, N.V. Thermal and mechanical stability of functionally graded carbon nanotubes (FG CNT)-reinforced composite truncated conical shells surrounded by the elastic foundations. Thin-Walled Structures. 2017. 115. Pp. 300–310. DOI: 10.1016/j.tws.2017.02.016
5. Kumar, S.K., Siddiraju, S. Effect of steel and polypropylene fiber on mechanical properties of concrete. International Journal of Civil Engineering and Technology. 2016. 7(3). Pp. 342–346.
6. Klyuev, S., Klyuev, A., Vatin, N. Fiber concrete for the construction industry. Magazine of Civil Engineering. 2018. 84(8). Pp. 41–47. DOI: 10.18720/MCE.84.4
7. Bespalov, V., Ucer, D., Salmanov, I., Kurbanov, I., Kupavykh, S. Deformation compatibility of masonry and composite materials. Magazine of Civil Engineering. 2018. 78(2). Pp. 136–150. DOI: 10.18720/MCE.78.11
8. Kanishchev, R. Analysis of local stability of the rectangular tubes filled with concrete. Magazine of Civil Engineering. 2016. 64(4). Pp. 59–68. DOI: 10.5862/MCE.64.6
9. Mashhadban, H., Kutanaei, S.S., Sayarinejad, M.A. Prediction and modeling of mechanical properties in fiber reinforced self-compacting concrete using particle swarm optimization algorithm and artificial neural network. Construction and Building Materials. 2016. 119. Pp. 277–287. DOI: 10.1016/j.conbuildmat.2016.05.034
10. Zhang, J., Zhang, M., Tang, W., Wang, W., Wang, M. Buckling of spherical shells subjected to external pressure: A comparison of experimental and theoretical data. Thin-Walled Structures. 2017. 111. Pp. 58–64. DOI: 10.1016/j.tws.2016.11.012
11. Godoy, L.A. Buckling of vertical oil storage steel tanks: Review of static buckling studies. Thin-Walled Structures. 2016. 103. Pp. 1–21. DOI: 10.1016/j.tws.2016.01.026
12. Yu, T., Yin, S., Bui, T.Q., Xia, S., Tanaka, S., Hirose, S. NURBS-based isogeometric analysis of buckling and free vibration problems for laminated composites plates with complicated cutouts using a new simple FSDT theory and level set method. Thin-Walled Structures. 2016. 101. Pp. 141–156. DOI: 10.1016/j.tws.2015.12.008
13. Timoshenko, S.P., Gere, J.M. Theory of Elastic Stability. Engineering Sociaties Monograps. McGrawHill, 1961. 541 p.
14. Szeidl, G. Effect of Change in Length on the Natural Frequencies and Stability of Circular Beams. PhD Thesis. Department of Mechanics. University of Miskolc, Hungary. 1975. (in Hungarian).
15. Simitses, G.J. An Introduction to the Elastic Stability of Structures. Prentice-Hall. Englewood Cliffs, 1976. 253 p.
16. Plaut, R.H. Snap-through of arches and buckled beams under unilateral displacement control. International Journal of Solids and Structures. 2015. 63. Pp. 109–113. DOI: 10.1016/j.ijsolstr.2015.02.044
17. Zhou, Y., Chang, W., Stanciulescu, I. Non-linear stability and remote unconnected equilibria of shallow arches with asymmetric geometric imperfections. International Journal of Non-Linear Mechanics. 2015. 77. Pp. 1–11. DOI: 10.1016/j.ijnonlinmec.2015.06.015
18. Han, Q., Cheng, Y., Lu, Y., Li, T., Lu, P. Nonlinear buckling analysis of shallow arches with elastic horizontal supports. Thin-Walled Structures. 2016. 109. Pp. 88–102. DOI: 10.1016/j.tws.2016.09.016
19. Tsiatas, G.C., Babouskos, N.G. Linear and geometrically nonlinear analysis of non-uniform shallow arches under a central concentrated force. International Journal of Non-Linear Mechanics. 2017. 92. Pp. 92–101. DOI: 10.1016/j.ijnonlinmec.2017.03.019

20. Abdelgawad, A., Anwar, A., Nassar, M. Snap-through buckling of a shallow arch resting on a two-parameter elastic foundation. Applied Mathematical Modelling. 2013. 37(16). Pp. 7953–7963. DOI: 10.1016/j.apm.2013.03.016
21. Liu, N., Plucinsky, P., Jeffers, A.E. Combining load-controlled and displacement-controlled algorithms to model thermal-mechanical snap-through instabilities in structures. Journal of Engineering Mechanics. 2017. 143(8). Article No. 04017051. DOI: 10.1061/(ASCE)EM.1943-7889.0001263
22. Lalin, V., Dmitriev, A., Diakov, S. Nonlinear deformation and stability of geometrically exact elastic arches. Magazine of Civil Engineering. 2019. 89(5). Pp. 39–51. DOI: 10.18720/MCE.89.4
23. Yan, S.-t., Shen, X., Chen, Z., Jin, Z. On buckling of non-uniform shallow arch under a central concentrated load. International Journal of Mechanical Sciences. 2017. 133. Pp. 330–343. DOI 10.1016/j.ijmecsci.2017.08.046
24. Yan, S.-t., Shen, X., Chen, Z., Jin, Z. Collapse behavior of non-uniform shallow arch under a concentrated load for fixed and pinned boundary conditions. International Journal of Mechanical Sciences. 2018. 137. Pp. 46–67. DOI: 10.1016/j.ijmecsci.2018.01.005
25. Yan, S.-t, Shen, X., Chen, Z., Jin, Z. On collapse of non-uniform shallow arch under uniform radial pressure. Engineering Structures. 2018. 160. Pp. 419–438. DOI: 10.1016/j.engstruct.2018.01.027
26. Yan, S.-t., Shen, X., Chen, Z., Jin, Z. Symmetric snap-through and equal potential energy load of non-uniform shallow arch under a concentrated load considering imperfection effect. International Journal of Mechanical Sciences. 2018. 146-147. Pp. 152–179. DOI: 10.1177/0954406219855105
27. Yan, S.-t., Shen, X., Jin, Z. Static and dynamic symmetric snap-through of non-uniform shallow arch under a pair of end moments considering critical slowing-down effect. Proceedings of the Institution of Mechanical Engineers, Part C: Journal of Mechanical Engineering Science. 2019. 233(16). Pp. 5735–5762. DOI: 10.1177/0954406219855105
28. Bateni, M., Eslami, M.R. Non-linear in-plane stability analysis of FGM circular shallow arches under central concentrated force. International Journal of Non-Linear Mechanics. 2014. 60. Pp. 58–69. DOI: 10.1016/j.ijnonlinmec.2014.01.001
29. Bateni, M. Eslami, M.R. Non-linear in-plane stability analysis of FG circular shallow arches under uniform radial pressure. Thin-Walled Structures. 2015. 94. Pp. 302–313. DOI: 10.1016/j.tws.2015.04.019
30. Babaei, H., Kiani, Y., Eslami, M.R. Thermomechanical nonlinear in-plane analysis of fix-ended FGM shallow arches on nonlinear elastic foundation using two-step perturbation technique. International Journal of Mechanics and Materials in Design. 2019. 15(2). Pp. 225–244. DOI: 10.1007/s10999-018-9420-y
31. Schreyer, H.L. The effect of initial imperfections on the buckling load of shallow circular arches. Journal of Applied Mechanics. 1972. 39(2). Pp. 445–450.
32. Plaut, R.H. Influence of load position on the stability of shallow arches. Zeitschrift für angewandte Mathematik und Physik ZAMP. 1979. 30(3). Pp. 548–552. DOI: 10.1007/BF01588902
33. Pi, Y.-L., Bradford, M.A., Liu, A. Nonlinear equilibrium and buckling of fixed shallow arches subjected to an arbitrary radial concentrated load. International Journal of Structural Stability and Dynamics. 2017. 17(8). Art. No. 1750082. DOI: 10.1142/S0219455417500821
34. Liu, A., Bradford, M.A., Pi, Y.-L. In-plane nonlinear multiple equilibria and switches of equilibria of pinned–fixed arches under an arbitrary radial concentrated load. Archive of Applied Mechanics. 2017. 87(11). Pp. 1909–1928. DOI: 10.1007/s00419-017-1300-7
35. Pi, Y.-L. Non-linear in-plane multiple equilibria and buckling of pin-ended shallow circular arches under an arbitrary radial point load. Applied Mathematical Modelling. 2020. 77. Pp. 115–136. DOI: 10.1016/j.apm.2019.07.021
36. Bradford, M.A., Uy, B., Pi, Y.-L. In-plane elastic stability of arches under a central concentrated load. Journal of Engineering Mechanics. 2002. 128(7). Pp. 710–719. DOI: 10.1061/(ASCE)0733-9399(2002)128:7(710)
37. Pi, Y.-L., Bradford, M. A. Dynamic buckling of shallow pin ended arches under a sudden central concentrated load. Journal of Sound and Vibration. 2008. 317. Pp. 898–917. DOI: 10.1016/j.jsv.2008.03.037
38. Kiss, L., Szeidl, G. In-plane stability of fixed-fixed heterogeneous curved beams under a concentrated radial load at the crown point. Technische Mechanik. 2015. 35(1). Pp. 31–48. DOI: 10.24352/UB.OVGU-2017-067
39. Kiss, L.P. Sensitivity of FGM shallow arches to loading imperfection when loaded by a concentrated radial force around the crown. International Journal of Non-Linear Mechanics. 2019. 116. Pp. 62–72. DOI: 10.1016/j.ijnonlinmec.2019.05.009
40. Kiss, L.P. Nonlinear stability analysis of fgm shallow arches under an arbitrary concentrated radial force. International Journal of Mechanics and Materials in Design. May 2019. DOI: 10.1007/s10999-019-09460-2
41. Kiss, L., Szeidl, G. Nonlinear in-plane stability of heterogeneous curved beams under a concentrated radial load at the crown point. Technische Mechanik. 2015. 35(1). Pp. 1–30. DOI: 10.24352/UB.OVGU-2017-066
42. Bateni, M., Eslami, M.R. Non-linear in-plane stability analysis of FGM circular shallow arches under central concentrated force. International Journal of Non-Linear Mechanics. 2014. 60. Pp. 58–69. DOI: 10.1016/j.ijnonlinmec.2014.01.001
43. Yan, S-t, Shen, X., Jin, Z. Instability of imperfect non-uniform shallow arch under uniform radial pressure for pinned and fixed boundary conditions. Thin-Walled Structures. 2018. 132. Pp. 217–236. DOI: 10.1016/j.tws.2018.08.018
44. Pi, Y.-L., Bradford, M.A., Tin-Loi F. Non-linear in-plane buckling of rotationally restrained shallow arches under a central concentrated load. International Journal of Non-Linear Mechanics. 2008. 43. Pp.1–17. DOI: 10.1016/j.ijnonlinmec.2007.03.013

Contacts:

Laszlo Peter Kiss, mechkiss@uni-miskolc.hu